Nanoporous film layers to enhance the performance of Passive Radiative Cooling paint mixtures

Giuseppe Emanuele Lio[1,2*], Sara Levorin[3], Atakan Erdoğan[3], Jeremy Werlé[1,2], Alain J. Corso[4], Luca Schenato[3], Diederik S. Wiersma[1,2,5], Marco Santagiustina[3], Lorenzo Pattelli[2,5], Maria Guglielmina Pelizzo[3,4]

[1*]Department of Physics, University of Florence, Vis Sansone 1, Sesto Fiorentino, 50019, Florence, Italy.
[2]European Laboratory for Non Linear Spectroscopy (LENS), University of Florence, Via Nello Carrara 1, Sesto Fiorentino, 50019, Florence, Italy.
[3]Dipartimento di Ingegneria dell'Informazione, Università di Padova, Via Gradenigo, 6/B, Padua, 35131, Italy.
[4]Consiglio Nazionale delle Ricerche - Istituto di Fotonica e Nanotecnologie (CNR-IFN), via Trasea, 7, Padua, 35131, Italy.
[5]Istituto Nazionale di Ricerca Metrologica (INRiM), Str. delle cacce, 91, Turin, 10135, Italy.

*Corresponding author(s). E-mail(s): giuseppeemanuele.lio@unifi.it;

Abstract

Passive radiative cooling (PRC) offers significant potential to reduce energy consumption and carbon emissions associated with cooling. Among various approaches, paint-like systems present several advantages in terms of cost-effectiveness, scalability, and ease of application. In this study, we report on a PRC system composed of a paint mixture modified with 50 % glass bubbles (GB) and a commercial polypropylene-polyethylene-polypropylene (PP-PE-PP) film, commonly used as a battery separator. The resulting material exhibits a solar reflectance of 94 % and a broad emittance of over 95 % in the sky-transparent window (STW) from 8 µm to 13 µm. The addition of glass bubbles enhances the solar reflectance of the base paint in the near-infrared wavelengths, while the nanoporous PP-PE-PP film (NPF) topcoat improves reflectance in the UV range, remains largely transparent in the IR, and renders the overall coating washable.

The material was tested under realistic outdoor conditions, comparing the performance when the PP-PE-PP film was directly applied onto the wet paint layer versus when it was used as a separate windshield enclosing the sample test chamber. Despite its high solar reflectance, no radiative cooling was observed relative to ambient temperature during peak hours (solar irradiation $>600\,\mathrm{W\,m^{-2}}$). However, below this threshold, a temperature drop of $-3\,^{\circ}\mathrm{C}$ and a cooling power exceeding $100\,\mathrm{W\,m^{-2}}$ were observed. Notably, even when a visibly opaque convection shield was used, the configuration in which the PP-PE-PP film sealed the sample slot resulted in significant overheating of the air pocket surrounding the sample during the day. This outcome suggests that experimental setups incorporating a windshield, commonly found in the literature, may introduce an artificial overheating effect, leading to biased measurements of passive radiative cooling

Keywords: Passive Radiative Cooling, Solar reflectance, Infrared emissivity, Temperature drop, Cooling power, Windshield

1 Introduction

Radiative cooling is a key technology that reduces the temperature of sky-facing objects through radiative energy transfer between the objects and outer space at 3 K [1]. For this reason, passive radiative cooling (PRC) holds promise as an electricity-free cooling strategy for dissipating heat of terrestrial objects through the atmospheric transparency window from 8 µm to 13 µm [2–7], and has attracted much attention for its potential of mitigating global warming [8] and the urban heat island effect [9]. Sub-ambient daytime cooling applications under direct sunlight illumination are particularly attractive and yet challenging to achieve [10, 11], requiring materials that are engineered to exhibit high reflectivity (larger than 95%) over the whole solar spectrum, combined with a high thermal emittance in the atmospheric transparency window ($\varepsilon \sim 1$) [12, 13]. The resulting daytime passive radiative cooling materials can undergo a spontaneous cooling process even during the day [14, 15], thus providing a net electricity-free cooling power [16–18]. A large interest in PRC materials moved has been directed towards paint-like coatings due to their application versatility and cost-effectiveness, using different mixtures of nano- and micro-particles such as $CaCO_3$, $BaSO_4$, BN or SiO_2 [19–23]. However, the extremely high particle densities typically associated with PRC paints require the use of toxic volatile organic solvents for their correct dispersion [24]. Additionally, materials such as $BaSO_4$ can lead to paint coatings with very high weight per unit area compared to typical paint formulations, which may limit their applicability and, consequently, their paint yield per square meter. To overcome the limitation posed by the restrictions on the overall Volatile Organic Compounds (VOCs) content of paints, recent efforts are being directed towards the development of water-based coatings [21, 25–27], which should also be sufficiently lightweight and durable. In this work, we propose a PRC system starting from a commercial water-based paint mixed with glass bubbles (GB) and covered with a nanoporous polypropylene-polyethylene-polypropylene (PP-PE-PP) film (NPF), acting as a hydrophobic barrier against both solar light (especially in the UV) and convection. Common nanoporous thin films have been explored as windshield protection in PRC experiments [28]; in this work, however, the NPF is directly applied onto the modified paint layer before it dries.

Convection is one of the main limitations in achieving sub-ambient temperatures, as reported by Zhen et al. [29]. In their work, a spectrally-selective emitter comprising silicon nitride, amorphous silicon, and an aluminum substrate was developed and enclosed with a vacuum-compatible ZnSe window. When shielded from direct sunlight, this surface achieved all-day cooling and a maximum sub-ambient temperature drop of 42 °C under vacuum conditions suppressing non-radiative heat-gains. The benefits associated to the use of vacuum chambers for passive radiative cooling demonstrations, such as achieving daytime sub-freezing temperatures as function of the surrounding pressure or suppressing parasitic heat fluxes and losses have been described by several groups in the recent literature [30–33]. A more common and easily implemented approach to mitigating convective exchanges, however, involves the use of thin films to shield emitters from direct wind, typically made of polyolefins such as polyethylene due to its transparency in the atmospheric window wavelength range [34, 35]. Different tests and optimizations have been reported in the past years to find favourable configurations and multi-functional convection shields. For instance, micro-structured polyethylene film fabricated through a scalable hot embossing lithography, leading to remarkable superhydrophobic properties [36]. Another attempt has been made using a nanoporous PE film as a windshield to enhance the radiative cooling of a PRC material, yet comparing the sample temperature to that of the enclosed micro-environment surrounding the sample [37]. Over the years, additional efforts have been made to explore the use of different polymeric windshields, both in direct contact with and separate from the PRC material [38]. Direct sunlight shields based on porous PE films were demonstrated, which exhibited a remarkable solar-weighted reflectivity up to 98 % combined with a maximum transmittance of 92 % in the sky transparency window [39–41]. Additional studies have been devoted to the possible role of PP as a slightly less IR-transparent but more durable alternative to PE [42]. Other previous attempts have been reported to vary the distance of the windshield from the PRC sample, showing appreciable differences between configurations [43]. In this work, we propose using the combined PP-PE-PP thin film as a cover layer directly applied to the PRC paint deposited above a compliant substrate. We explore two different metallic substrates with different reflectivity in the VIS spectrum of 90 % (S90-substrate) and 95 % (V95-substrate). Both approaches, which consist of sticking the PP-PE-PP film directly onto the wet paint layer or using it as a separate windshield enclosing the test chamber, have been evaluated in terms of temperature drop and net cooling power, returning equivalent results at a sufficiently high thickness of the composite coating layer.

2 Materials and Method

2.1 Sample preparation

The proposed PRC samples have been prepared by mixing a commercial water-based paint (Exterieur by ThermoShield, currently under the ClimateCoating brand) with low VOCs $\leq 3\,\mathrm{g\,L^{-1}}$ containing titanium dioxide, zinc oxide, kaolin, calcium carbonate, silicates and water [44] with the 3M GB IM30K (25 %) in weight and 25 % of water (Figure 1a). Then, the prepared paint was applied using a brush on two different aluminium substrates (V95 and S90, Almeco S.p.A., Italy). The paint application step was repeated up to four times to manufacture samples with increasing thickness. Finally, the nanoporous film (NPF) was incorporated into the final paint layer before drying. This film is a 16 µm-microporous trilayer membrane composed of polypropylene, polyethylene, and polypropylene (C210, Celgard, USA). As illustrated in Figure 1c, the thin film was applied over the wet paint using a roller, smoothing its surface and flattening the typical texture left by the brush. Figure 1d provides a schematic illustration of the incoming solar radiation and the final PRC sample, which includes the nanoporous PP-PE-PP film. Once manufactured, the thickness of the PRC sam-

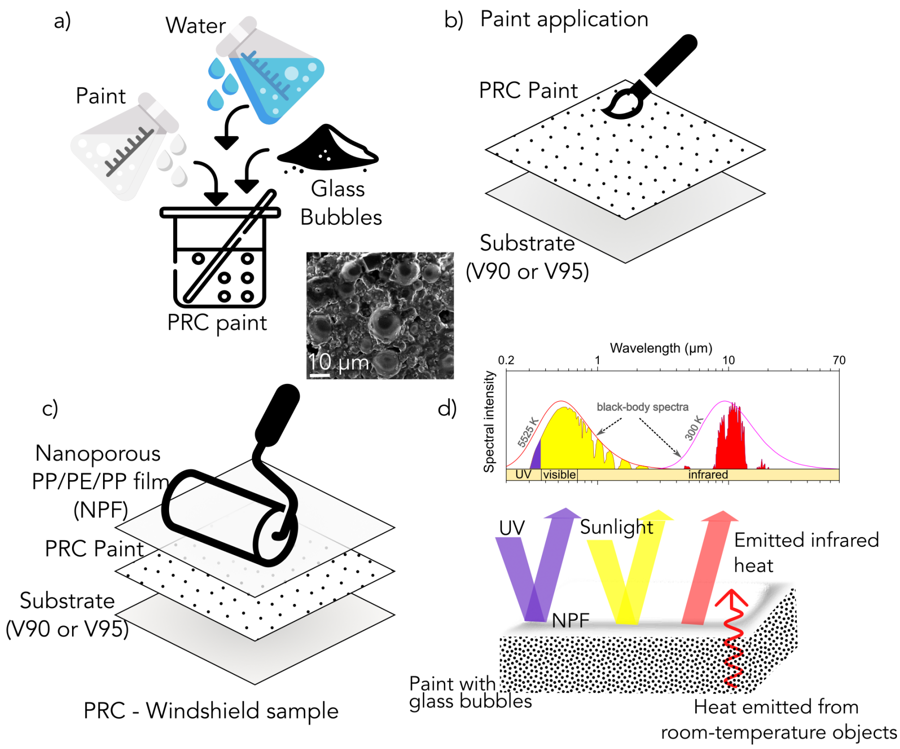

Fig. 1 a) Schematic representation of the PRC paint preparation, b) it is applied using a brush on the two metallic substrates, namely S90 and V95. c) A roller applies the NPF to the PRC paint. d) sketch of the sample and its working principle for spontaneous radiative cooling (readapted from Wikimedia).

ples was measured by a Tesa Digital Caliper 05.30080 with an accuracy of ±0.02 mm by substracting the known thickness of the metal substrate. Coating thicknesses of 0.14 mm, 0.32 mm, 0.47 mm, and 0.74 mm were obtained for 1-4 coats with NPF for the V95 substrate, respectively. For the S90 substrate, thicknesses of 0.15 mm, 0.21 mm, 0.66 mm, and 0.96 mm were obtained for 1-4 coats with NPF, respectively. The bare substrates and the PRC samples were characterized optically with a Cary 5000 UV-VIS-NIR (Agilent, USA), equipped with a double-grating spectrophotometer using the internal diffuse reflectance accessory at $3°20'$ angle of incidence with an accuracy better than 2 %.

2.2 Experimental apparatus

The outdoor tests aimed at evaluating the PRC material's temperature drop and net cooling power have been performed using the samples with three paint coats applied on the V95 substrate. Two pairs of samples are compared, each with three paint layers, plus the NPF film either directly applied onto the paint, or used as a separate convection shield enclosing the sample slot aperture. Outdoor measurements were carried out using the experimental setup described in [13], which includes:

- a professional PVC Stevenson shield (Radiation Shield - SKU 7714 by Davis, USA [45]);
- multiple DHT22 sensor modules [46] for simultaneous ambient temperature and relative humidity measurements. The accuracy of these temperature probes is ±0.5 °C for the temperature and ±2 % for the relative humidity measurements; One DHT22 probe is placed inside the professional Stevenson Shield (which is identified as T_{amb}), while the other two available DHT22 are used as additional references.
- multiple Negative Temperature Coefficient (NTCs) model 103JT-025 of 10 kΩ (Transfer Multisort Elektronik, IT [47]) to measure the samples temperature;
- a BH1750 (Rohm semiconductor LTD, UK [48]) light sensor monitoring solar irradiance;
- an IR temperature sensor (MLX90614ESF-BCF-000-TU, Melexis, Inc., USA [49]) to track the apparent sky temperature.

The temperature and solar irradiance data are regulated using as a reference the data of a nearby weather station operated by the LaMMA consortium between the National Research Council of Italy (CNR) and the Tuscany region [50]. Additionally, to evaluate the net cooling power, a Proportional-Integral-Derivative (PID) controller is fed with ambient temperature readings, which are then used to drive a resistive heater [13]. Figure 2a depicts the experimental test box used for the T_{drop} and P_{cool} measurements. The sample holder is manufactured from an expanded polystyrene (EPS) parallelepiped with dimensions 20 cm × 14 cm × 75 cm (h×w×l). These dimensions allow to accommodate four 6 cm × 6 cm samples arranged equidistantly from each other. The samples are then held in position with a EPS lid with a height of 0.5 cm and four apertures to host them. The EPS lid is coated with a highly diffuse reflective tape (3M, USA), while the lateral walls of the EPS base are wrapped in aluminum foil. Note that this setup allows for simultaneously measuring both T_{drop} and P_{cool} using a pair of identical samples in parallel, which is important to compare and characterize passive radiative cooling materials under the same environmental conditions [51]. Figure 2a shows the two tested configurations arranged in the T_{drop} and P_{cool} measurement areas. In the first configuration, dubbed as "enclosed", the NPF is used to seal the slot where the paint sample is located, shielding it from external air. In the second configuration, which we refer to as "open", the NPF is directly applied onto the paint layer. Hence, external air is free to circulate in the slot and around the sample. In this setup, temperature measurements are taken both directly in contact with the sample substrate (S1 "enclosed", S2 "open") and underneath it (U.S1 "enclosed", U.S2 "open"). In both cases the NTCs in position U.S1 and U.S2 are used to monitor the temperature beneath the samples and to assess if the thin air surrounding the sample exhibits any significant warming during daytime hours. Additionally, another NTC was placed under the lid. This measurement serves as an additional reference to ensure the EPS block holding the samples does not overheat, which could interfere with the spontaneous cooling of the samples. In particular, this extra parameter offers a way to determine the potential impact of the sample holder on the cooling performance. On the other hand, for the simultaneous P_{cool} experiment, the NTCs and the heaters are placed in direct contact with the samples as depicted by P.S1 and P.S2, respectively. Figure 2b shows a top view of the setup identifying the described test areas.

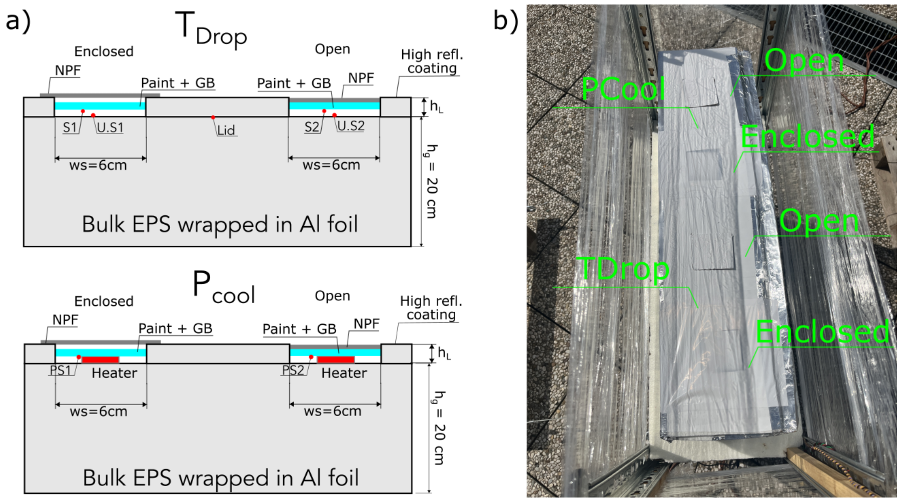

Fig. 2 a) Sketch with the dimensions of the experimental sample holder, the samples, the NTCs, and heaters arrangement. The sample width (ws) is 6 cm, the lid height (h_{L}) is 0.5 cm and the height of the bulk EPS (h_{g}) is 20 cm. The top panel illustrates the T_{drop} and the bottom panel reports the P_{cool} test areas, as well as the enclosed and open configurations, respectively. b) Top view of the actual setup identifying the test areas and conditions.

3 Results

3.1 Optical characterization

The results of the optical characterization are reported in Figure 3a for the V95 substrate in blue in the range 250 and 2500 nm. The solid red line shows the reflectance of the Exterieur ThermoShield paint used as the base for the mixture. The light-orange solid line correspond to the paint with the glass bubbles applied on the V95. The violet solid line corresponds to the reflectivity of the NPF, which presents high reflectance in the UV region (75 %) of the spectrum along with a moderate and high transmittance in the VIS-NIR spectrum (10 % at 2000 nm). This fact supports the utility of applying this film as the final layer of the proposed system. The same characterization has been performed on the S90 substrate and reported in Figure A1a in the Appendix. Figure 3b shows the reflectance of the composite paint + NPF system with multiple

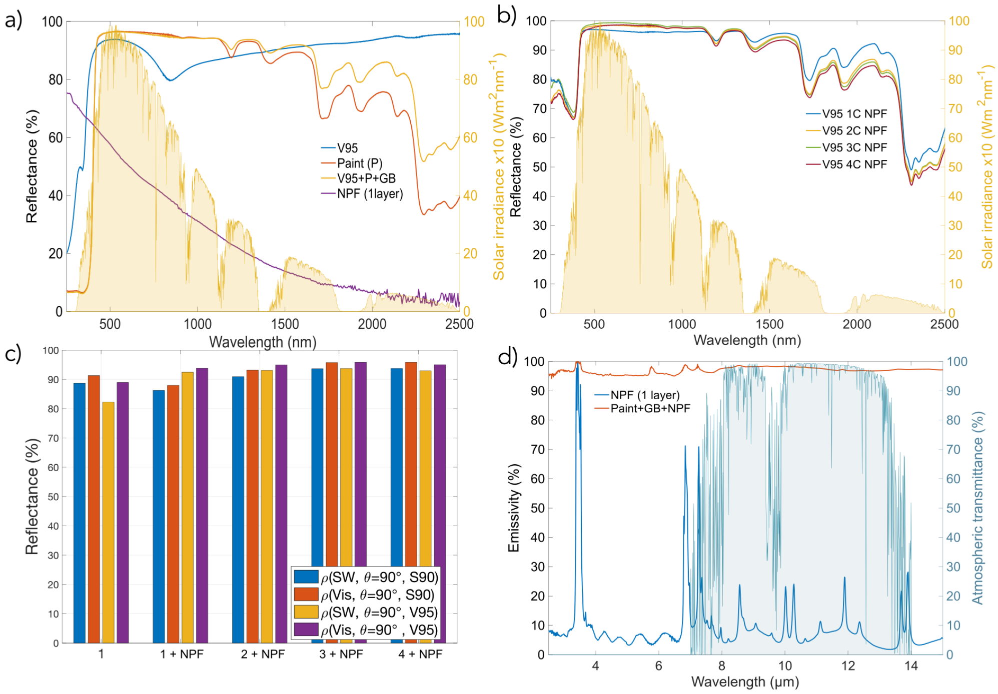

Fig. 3 a) Reflectances for: V95 substrate, pristine paint, paint with GB and NPF. b) The V95 substrate has been covered with an increasing number of paint coats with the NPF applied to their top. In both previous panels the second y axis refers to the ASTM G173 solar irradiance. c) Bar chart reporting the total solar and visible reflectance of (1) the paint + GB, and (1-4 + NPF) the increasing number of paint + GB coats covered with the NPF applied on V90 and V95. d) The emissivity measured by FTIR for a single layer of NPF (blue solid line) and the paint + GB + NPF (orange solid line).

paint layers (up to four) applied on the V95 substrate. The same characterization for the S90 substrate and the free-standing samples are reported in Figure A1b and c in Appendix. Noticeably, all samples show a larger reflectance compared to those without the NPF topcoat. In particular, samples with up to 2 coating-layers surpass the 95 % in the wavelength range (400 and 1200 nm). Above 3 layers of paint (corresponding to thicknesses of about 50-60 µm) with the NPF top coat results in almost identical reflectance. Figures A2a,b in the Appendix report the reflectance, transmittance and absorbance (emissivity) of the NPF layer characterized across solar and IR spectrum.

The bar charts of Figure 3c report the solar (SW)-and VIS-weighted hemispherical reflectance of the samples for a different number of paint coats with GB and NPF applied on both substrates. Solar-weighted hemispherical reflectance was calculated by normalizing the absolute reflectivity of each sample by the solar spectrum ASTM G173 [52, 53], as:

$$\rho([\mathrm{SW,Vis}], \theta, h) = \frac{\sum_{\lambda} \rho_h(\lambda, \theta, h) E_{\lambda}(\lambda) \Delta\lambda}{\sum_{\lambda} E_{\lambda}(\lambda) \Delta\lambda}, \tag{1}$$

where $\rho_h(\lambda, \theta, h)$ is the average hemispherical reflectance spectrum measured for each sample (identified by h), and $E_{\lambda}(\lambda)$ the solar irradiance spectrum for the wavelength intervals of $\Delta\lambda = 1\,\mathrm{nm}$, and $\theta = 90°$ is the incidence angle. In particular, the solar-weighted hemispherical reflectance $\rho(\mathrm{SW}, \theta, h)$ was determined for wavelengths between 280 and 2650 nm; the VIS-weighted hemispherical reflectance $\rho(\mathrm{Vis}, \theta, h)$ was calculated for wavelengths from 380 nm to 750 nm. The results reported in Figure 3c show that the reflectance of the coated samples becomes largely independent of the choice of the substrate above three coating layers. Finally, Figure 3d shows the emissivity measured for the paint + GB + NPF and the NPF layer. The data has been collected using a Cary 630 FTIR (Fourier Transform Infrared Spectroscopy, Agilent, USA) over the IR range (2.5 µm to 15 µm). In this graph, the blue solid line refers to the NPF layer alone, while the orange solid line refers to the sample made by one coat of Paint + GB and the NPF applied on top. The paint formulation shows a broad and higher emissivity across the sky transparency window (STW) range, with visible features associated to the presence of glass bubbles [54] showing absorption peaks at 8.5 µm, 9.76 µm, 12.4 µm [55], corresponding to resonances associated to the Si-O-Si bond. On the other hand, the analysis shows O-H and C-H bonds from 3.0 µm to 4.0 µm, a peak at 5.7 µm from the resin binder used in acrylic paint (methyl methacrylate, $CH_2{=}C(CH_3)COOCH_3$), while the NPF is identified by C-CH_3 (6.8 µm), -CH (7.2 µm), and C-C (11.8 µm) bonds [56–58], further details about the FTIR analysis are reported in Figure A3 in Appendix. Considered separately, the isolated NPF film has an overall absorbance lower than 10 % in the same range. Due to its fine morphological and optical features, this film enhances reflectance at UV wavelenghts (Figure 3a,b). At the same time, its IR transparency facilitates radiative exchange towards outer space through the STW (see Figure A2b). Therefore, these results confirm the advantage of covering a high emissivity paint with an IR transparent layer to boost the low UV reflectance of the bare ThermoShield paint (see Figure 3b) without impairing its infrared emittance.

3.2 Outdoor tests

Figure 4 presents the measurements collected over three consecutive days using the setup shown in Figure 2. Figure 4a shows the ambient temperature measured in the Stevenson Shield (T_{amb}), alongside with the temperature of the sample shielded by the NPF (S1, enclosed), of the sample with NPF as the top layer (S2, open), of the air gap below S1 (U.S1) and S2 (U.S2), and of the gap between the EPS lid and the EPS base block (T_{Lid}). Figure 4b displays the environmental data, including relative humidity, solar irradiance, and sky temperature (T_{sky}). Figure 4c illustrates the temperature differences (ΔT) for S1 and S2, while Figure 4d shows the ΔT values for U.S1, U.S2, and under the lid, all calculated relative to the external ambient temperature. The right axis in these plots corresponds to solar irradiance. The plot shows that sub-ambient temperatures for S1 and S2 are achieved when solar irradiance falls below $600\,\mathrm{W\,m^{-2}}$, while the sensors below the samples reach this condition only below $430\,\mathrm{W\,m^{-2}}$. Notably, during peak irradiance, the enclosed sample (S1) reaches a significantly higher temperatures than the open sample (S2) where the NPF is directly applied to the paint. Figure 4e tracks sample temperatures during P_{cool} measurements, while Figure 4f shows the net cooling power for both configurations. Despite the lower nighttime temperatures in the enclosed setup, its corresponding cooling power is also slightly lower due to the better heat retention within the enclosed air pocket. When the sky temperature (T_{sky}) drops below $5\,^{\circ}\mathrm{C}$, cooling power is found to exceed $100\,\mathrm{W\,m^{-2}}$. A condensed overview of the data can be obtained from the violin plots of Figure 5.

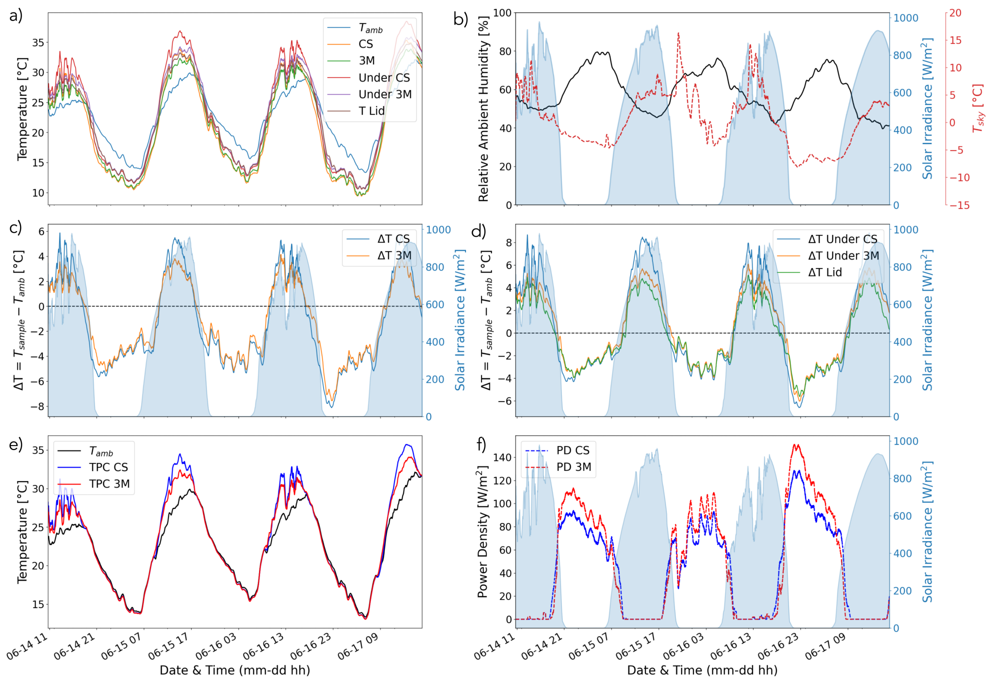

Fig. 4 a) Ambient temperature and sample temperatures for the enclosed (S1) and open (S2) conditions, including temperatures under both samples and the lid that covers the EPS sample holder. b) Relative ambient humidity, solar irradiance, and sky temperature as a proxy to the presence of clouds. c) Temperature difference ΔT calculated as the difference between the S1 and S2 temperature and ambient. d) Temperature difference ΔT calculated as the difference between the temperature under S1, S2 and lid and ambient. e) Sample temperature for enclosed and open conditions monitored during the P_{cool} measurement, using external ambient temperature as the set point; f) Net cooling power measured for both configurations.

The ΔT of the enclosed and open configurations are represented and compared in

Figure 5a, with reference to morning (5-11), midday (11-17), afternoon (17-23), and night (23-5) hours. As one can note, in all the periods except midday, the two configurations show similar behavior, with a larger spread of ΔT during the afternoon. At midday, the two configurations show the most significant ΔT, yet with a different spread. Within this time window, the enclosed sample experiences overheating peaks up to 6 °C above ambient temperature, more than 2 °C larger than the open configuration. Similar conclusions can be drawn from the temperature difference ΔT U.S1 (enclosed) and U.S2 (open) measured below the samples and represented in Figure 5b. In particular, a temperature difference peak of more than 8 °C is reached at midday for U.S1 (enclosed), which is more than 3 °C larger than that the maximum U.S2 (open) reading.

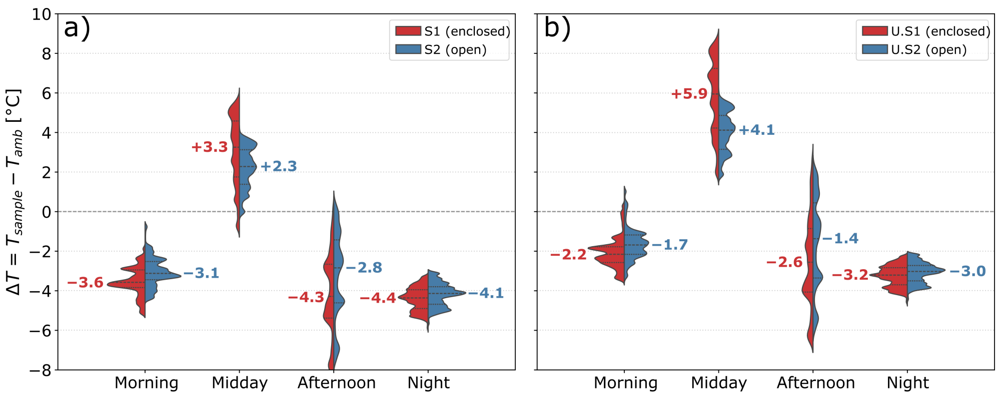

Fig. 5 Split violin plot comparing the temperature difference ΔT for the following conditions: a) enclosed (S1) versus open (S2) sample and b) under the S1 and S2 samples. The values reported next to each distribution represent the median calculated for each time window over the three-day observation period.

Finally, the median temperature for each configuration over the three days of measurements is reported in the violin plots (Figure 5) showing the marked difference observed during the day, and the opposite trend registered in the evening, where the cooled air pocket helps maintaining a sub-ambient temperature in the enclosed configuration.

4 Conclusion

In this work, we proposed a low-VOC ($\leq$ 3 %) paint containing glass bubbles and a thin layer of nanoporous PP-PE-PP film directly applied on top. The proposed coating, which is realized using commercially available components, can reach a solar weighted reflectance of 94 % and an emittance of 95 % after three coats on an aluminum substrate. Part of its cooling performance is endowed by the direct inclusion of an IR-transparent topcoat, which makes the paint washable, shields it from contamination, and contributes to reflecting a large part of the UV spectrum that would be otherwise absorbed by the commercial base paint formulation. Two different configurations, consisting of a bare paint coating placed in a slot enclosed by the NPF membrane, and one with the NPF directly applied on top of the paint formulation, have been tested outdoors. For daytime cooling applications, the results highlight the benefit of integrating the nanoporous PP-PE-PP thin layer into the material, showing a median temperature reduction in midday of $1\,^{\circ}\mathrm{C}$ compared to the case where the same NPF cover is used as a conventional solar and wind shield. The proposed PRC material demonstrates median temperature drops around $-3\,^{\circ}\mathrm{C}$ during the daytime when solar irradiance is below $600\,\mathrm{W\,m^{-2}}$. At night, it achieves a maximum temperature drop of about $-7\,^{\circ}\mathrm{C}$. The net cooling power reaches up to $120\,\mathrm{W\,m^{-2}}$ for the PRC sample in the enclosed slot and up to $140\,\mathrm{W\,m^{-2}}$ for the sample with the NPF layer applied on its top. Other features, such as adhesion strength and environmental robustness, are crucial for the commercial application of new PRC materials. Although these factors were not addressed in this study, they will be the focus of future investigations. The proposed experiments show how the contribution of the NPF foil can vary during the different time of the day. During peak irradiation hours, a lower sample temperature is obtained with the NPF applied directly onto the paint, with air circulating freely around the sample, which stands in contrast with the prevalent use of windshields in the literature. The reason why this contrast is not apparent in previous works, is that most papers use a reference "ambient" temperature taken inside the enclosed air pocket. This bias is reversed in the remaining part of the day (which is often not reported in many recent papers, focusing only on the central hours of the day). Our results show that the typical use of IR-transparent convection shields to seal the test slots hosting the samples can lead to an undesired "greenhouse" effect obliterating the sought cooling. This effect is still relevant even when using partially reflecting porous films, despite the additional sun shielding that they provide. This effect should be kept into account by researchers, depending on the targeted application (daytime or nighttime cooling). At the same time, care should be taken as to not use a reference ambient temperature measurement inside such enclosed air pockets, as this would lead to a significant over-estimation of the temperature drop achieved by the emitter.

5 Author contributions:

G.E.L, J.W., L.P. prepared the samples and built the outdoor experimental apparatus. S.L, A.E, L.S, M.S and M.G.P. performed the optical and morphological characterization. A.J.C. and M.G.P. curated the optical characterization data. D.S.W. and L.P. provided indications on the methodology. All authors contributed to writing and revising the paper. L.P. and M.G.P. supervised the project.

6 Funding:

This work was supported by the European project PaRaMetriC, code 21GRD03 and the "FSE-REACT EU" program financed by National Social Fund–National Operative Research Program and Innovation 2014-2020.

7 Acknowledgements:

The authors thank Roberto Concas for technical support during the preparation of the measurement apparatus, and the members of PaRaMetriC for support with the characterization of the NPF film. Part of this work is supported by the European project PaRaMetriC, code 21GRD03. The project 21GRD03 PaRaMetriC received funding from the European Partnership on Metrology, co-financed by the European Union's Horizon Europe Research and Innovation Programme and from the Participating States. G.E.L. acknowledges support from the "FSE-REACT EU" program financed by National Social Fund–National Operative Research Program and Innovation 2014-2020 (D.M. 1062/2021), personal Grant number 10-G-15049-2. J.W. acknowledges co-funding by the European Union - PON Research and Innovation 2014-2020 in accordance with Article 24, paragraph 3a), of Law No. 240 of December 30, 2010, as amended, and Ministerial Decree No. 1061 of August 10, 2021.

8 Data availability:

A dataset containing the outdoor measurements and the sample characterization are available at https://doi.org/10.5281/zenodo.13938561

References

[1] Raman, A.P., Anoma, M.A., Zhu, L., Rephaeli, E., Fan, S.: Passive radiative cooling below ambient air temperature under direct sunlight. Nature **515**(7528), 540–544 (2014)

[2] Li, D., Liu, X., Li, W., Lin, Z., Zhu, B., Li, Z., Li, J., Li, B., Fan, S., Xie, J., *et al.*: Scalable and hierarchically designed polymer film as a selective thermal emitter for high-performance all-day radiative cooling. Nature Nanotechnology **16**(2), 153–158 (2021)

[3] Yin, X., Yang, R., Tan, G., Fan, S.: Terrestrial radiative cooling: Using the cold universe as a renewable and sustainable energy source. Science **370**(6518), 786–791 (2020)

[4] Zhu, B., Li, W., Zhang, Q., Li, D., Liu, X., Wang, Y., Xu, N., Wu, Z., Li, J., Li, X., *et al.*: Subambient daytime radiative cooling textile based on nanoprocessed silk. Nature nanotechnology **16**(12), 1342–1348 (2021)

[5] Cho, J.-W., Lee, E.-J., Kim, S.-K.: Radiative cooling technologies: a platform for passive heat dissipation. Journal of the Korean Physical Society **81**(6), 481–489 (2022)

[6] Liu, S., Sui, C., Harbinson, M., Pudlo, M., Perera, H., Zhang, Z., Liu, R., Ku, Z., Islam, M.D., Liu, Y., *et al.*: A scalable microstructure photonic coating fabricated by roll-to-roll "defects" for daytime subambient passive radiative cooling. Nano Letters **23**(17), 7767–7774 (2023)

[7] Li, X., Ding, Z., Kong, L., Fan, X., Li, Y., Zhao, J., Pan, L., Wiersma, D.S., Pattelli, L., Xu, H.: Recent progress in organic-based radiative cooling materials: fabrication methods and thermal management properties. Materials Advances **4**(3), 804–822 (2023)

[8] Burke, M., Hsiang, S.M., Miguel, E.: Global non-linear effect of temperature on economic production. Nature **527**(7577), 235–239 (2015)

[9] Wang, J., Sun, J., Guo, T., Zhang, H., Xie, M., Yang, J., Jiang, X., Chu, Z., Liu, D., Bai, S.: High-strength flexible membrane with rational pore architecture as a selective radiator for high-efficiency daytime radiative cooling. Advanced Materials Technologies **7**(1), 2100528 (2022)

[10] Jing, W., Zhang, S., Zhang, W., Chen, Z., Zhang, C., Wu, D., Gao, Y., Zhu, H.: Scalable and flexible electrospun film for daytime subambient radiative cooling. ACS Applied Materials & Interfaces **13**(25), 29558–29566 (2021)

[11] Ding, Z., Li, X., Zhang, H., Yan, D., Werlé, J., Song, Y., Pattelli, L., Zhao, J., Xu, H., Li, Y.: Robust radiative cooling via surface phonon coupling-enhanced emissivity from sio2 micropillar arrays. International Journal of Heat and Mass Transfer **220**, 125004 (2024)

[12] Kim, H., McSherry, S., Brown, B., Lenert, A.: Selectively enhancing solar scattering for direct radiative cooling through control of polymer nanofiber morphology. ACS Applied Materials & Interfaces **12**(39), 43553–43559 (2020)

[13] Lio, G.E., Werlé, J., Arduini, M., Wiersma, D.S., Manara, J., Pattelli, L.: Radiative cooling potential of a water-based paint formulation under realistic application conditions. ACS Applied Optical Materials (2024)

[14] Hossain, M.M., Gu, M.: Radiative cooling: principles, progress, and potentials. Advanced Science **3**(7), 1500360 (2016)

[15] Sui, C., Hsu, P.-C.: Standardizing the thermodynamic definition of daytime subambient radiative cooling. ACS Energy Letters **9**, 2997–3000 (2024)

[16] Miller, J.L.: Passive cooling doesn't cost the planet. Physics today **70**(4), 16–18 (2017)

[17] Chu, S., Cui, Y., Liu, N.: The path towards sustainable energy. Nature materials **16**(1), 16–22 (2017)

[18] Ding, Z., Li, H., Li, X., Fan, X., Jaramillo-Fernandez, J., Pattelli, L., Zhao, J., Niu, S., Li, Y., Xu, H.: Designer sio2 metasurfaces for efficient passive radiative cooling. Advanced Materials Interfaces, 2300603 (2023)

[19] Atiganyanun, S., Kumnorkaew, P.: Effects of pigment volume concentration on

radiative cooling properties of acrylic-based paints with calcium carbonate and hollow silicon dioxide microparticles. International Journal of Sustainable Energy **42**(1), 612–626 (2023)

[20] Li, X., Peoples, J., Huang, Z., Zhao, Z., Qiu, J., Ruan, X.: Full daytime sub-ambient radiative cooling in commercial-like paints with high figure of merit. Cell Reports Physical Science **1**(10), 1–12 (2020)

[21] Huang, W., Chen, Y., Luo, Y., Mandal, J., Li, W., Chen, M., Tsai, C.-C., Shan, Z., Yu, N., Yang, Y.: Scalable aqueous processing-based passive daytime radiative cooling coatings. Advanced Functional Materials **31**(19), 2010334 (2021)

[22] Du, T., Niu, J., Wang, L., Bai, J., Wang, S., Li, S., Fan, Y.: Daytime radiative cooling coating based on the y2o3/tio2 microparticle-embedded pdms polymer on energy-saving buildings. ACS Applied Materials & Interfaces **14**(45), 51351–51360 (2022)

[23] Felicelli, A., Katsamba, I., Barrios, F., Zhang, Y., Guo, Z., Peoples, J., Chiu, G., Ruan, X.: Thin layer lightweight and ultrawhite hexagonal boron nitride nanoporous paints for daytime radiative cooling. Cell Reports Physical Science **3**(10), 1–17 (2022)

[24] Li, X., Peoples, J., Yao, P., Ruan, X.: Ultrawhite baso4 paints and films for remarkable daytime subambient radiative cooling. ACS Applied Materials & Interfaces **13**(18), 21733–21739 (2021)

[25] Xue, X., Qiu, M., Li, Y., Zhang, Q., Li, S., Yang, Z., Feng, C., Zhang, W., Dai, J.-G., Lei, D., *et al.*: Creating an eco-friendly building coating with smart subambient radiative cooling. Advanced Materials **32**(42), 1906751 (2020)

[26] Zhao, Y., Pang, D., Chen, M., Chen, Z., Yan, H.: Scalable aqueous processing-based radiative cooling coatings for heat dissipation applications. Applied Materials Today **26**, 101298 (2022)

[27] Gong, Q., Lu, L., Chen, J., Lau, W.Y., Cheung, K.H.: A novel aqueous scalable eco-friendly paint for passive daytime radiative cooling in sub-tropical climates. Solar Energy **255**, 236–242 (2023)

[28] Hsu, P.-C., Song, A.Y., Catrysse, P.B., Liu, C., Peng, Y., Xie, J., Fan, S., Cui, Y.: Radiative human body cooling by nanoporous polyethylene textile. Science **353**(6303), 1019–1023 (2016)

[29] Zhen, C., Zhu, L., Raman, A., Fan, A.: Radiative cooling to deep sub-freezing temperatures through a 24-h day–night cycle. Nat. Commun. **7**(1), 13729 (2016)

[30] Tso, C.Y., Chan, K.C., Chao, C.Y.: A field investigation of passive radiative cooling under hong kong's climate. Renewable energy **106**, 52–61 (2017)

[31] Chen, Z., Zhu, L., Li, W., Fan, S.: Simultaneously and synergistically harvest energy from the sun and outer space. Joule **3**(1), 101–110 (2019)

[32] Hu, M., Zhao, B., Cao, J., Wang, Q., Riffat, S., Su, Y., Pei, G., *et al.*: Effect of vacuum scheme on radiative sky cooling performance. Applied Thermal Engineering **219**, 119657 (2023)

[33] Banik, U., Meddeb, H., Berends, D., Reininghaus, N., Sergeev, O., Busch, L., Gehrke, K., Vehse, M., Agert, C.: Impact of parasitic heat fluxes on deep sub-ambient radiative coolers under variable pressure. Applied Thermal Engineering **237**, 121655 (2024)

[34] Zhang, J., Yuan, J., Liu, J., Zhou, Z., Sui, J., Xing, J., Zuo, J.: Cover shields for sub-ambient radiative cooling: A literature review. Renewable and Sustainable Energy Reviews **143**, 110959 (2021)

[35] Cho, J.-W., Yoon, S.-S., Lee, E.-J., Kim, S.-K.: Anti-greenhouse effect via regulation of surface emissivity. IEEE Photonics Journal **14**(2), 1–7 (2022)

[36] Jiang, Y., Wang, J., Zhou, Y., Li, J., Chen, Z., Yao, P., Ge, H., Zhu, B.: Micro-structured polyethylene film as an optically selective and self-cleaning layer for enhancing durability of radiative coolers. Nanophotonics **12**(12), 2213–2220 (2023)

[37] Gao, Y., Song, X., Zhang, P.: Comprehensive evaluation and analysis of a porous polymer coating for highly efficient passive radiative cooling. Solar Energy Materials and Solar Cells **250**, 112081 (2023)

[38] Liu, J., Tang, H., Zhang, J., Zhang, D., Jiao, S., Zhou, Z.: Boosting daytime radiative cooling performance with nanoporous polyethylene film. Energy and Built Environment **4**(2), 131–139 (2023)

[39] Cao, D., Li, X., Gu, Y.: Highly optically selective polyethylene porous films as versatile optical shields for daytime radiative cooling applications. Solar Energy Materials and Solar Cells **240**, 111727 (2022)

[40] Liu, J., Zhang, D., Jiao, S., Zhou, Z., Zhang, Z., Gao, F.: Daytime radiative cooling with clear epoxy resin. Solar Energy Materials and Solar Cells **207**, 110368 (2020)

[41] Torgerson, E., Hellhake, J.: Polymer solar filter for enabling direct daytime radiative cooling. Solar Energy Materials and Solar Cells **206**, 110319 (2020)

[42] Martorell, I., Camarasa, J., Vilà, R., Solé, C., Castell, A.: Aging study of plastics to be used as radiative cooling wind-shields for night-time radiative cooling—polypropylene as an alternative to polyethylene. Energies **15**(22), 8340 (2022)

[43] Cho, J.-W., Chang, S.-K., Park, S.-J., Oh, S., Nam, Y., Kim, S.-K.: Switching of heating and cooling modes using thermal radiation films. Current Applied Physics **20**(9), 1073–1079 (2020)

[44] ThermoShield Paint datasheet. https://img1.wsimg.com/blobby/go/0a057b5a-cb5c-4931-aafe-4d5394f11f27/downloads/TB-TS-Exterieur.pdf?ver=1705925819259

[45] Davis instruments - User Manual. https://cdn.shopify.com/s/files/1/0515/5992/3873/files/07395-093_IM_07714.pdf

[46] DHT22 - Ambient temperature and relative humidity sensor - DataSheet. http://cdn.sparkfun.com/datasheets/Sensors/Weather/RHT03.pdf

[47] Negative Temperature Coefficient (NTC) thermistors, model: 103JT-025. DataSheet. https://www.tme.eu/Document/85c74588be813b44821ab28dae36c629/TT6-10KC8-9-25.pdf

[48] BH1750 Light sensor DataSheet. https://mm.digikey.com/Volume0/opasdata/d220001/medias/docus/6165/bh1750fvi-e.pdf

[49] Melexis MLX90614 DataSheet. https://www.melexis.com/-/media/files/documents/datasheets/mlx90614-datasheet-melexis.pdf

[50] LaMMA Webpage. https://www.lamma.toscana.it/meteo/osservazioni-e-dati/dati-stazioni

[51] Fan, F., Xu, D., Zhu, Y., Tan, G., Zhao, D.: A simple, accurate, and universal method for characterizing and comparing radiative cooling materials and devices. International Journal of Heat and Mass Transfer **200**, 123494 (2023)

[52] Green, M.A.: Limiting photovoltaic efficiency under new astm international g173-based reference spectra. Progress in Photovoltaics: Research and Applications **20**(8), 954–959 (2012)

[53] Kim, M., Seo, J., Yoon, S., Lee, H., Lee, J., Lee, B.J.: Optimization and performance analysis of a multilayer structure for daytime radiative cooling. Journal of Quantitative Spectroscopy and Radiative Transfer **260**, 107475 (2021)

[54] Sun, Y., He, H., Huang, X., Guo, Z.: Superhydrophobic sio2–glass bubbles composite coating for stable and highly efficient daytime radiative cooling. ACS Applied Materials & Interfaces **15**(3), 4799–4813 (2023)

[55] Lee, S.-J., Kim, G.-M., Kim, C.-L.: Design and evaluation of micro-sized glass bubble embedded pdms composite for application to haptic forceps. Polymer Testing **117**, 107855 (2023)

[56] Chu, P.M., Guenther, F.R., Rhoderick, G.C., Lafferty, W.J.: The nist quantitative

infrared database. Journal of research of the National Institute of Standards and Technology **104**(1), 59 (1999)

[57] Nakamoto, K.: Infrared and Raman Spectra of Inorganic and Coordination Compounds, Part B: Applications in Coordination, Organometallic, and Bioinorganic Chemistry. John Wiley & Sons, ??? (2009)

[58] Zhou, L., Rada, J., Tian, Y., Han, Y., Lai, Z., McCabe, M.F., Gan, Q.: Radiative cooling for energy sustainability: Materials, systems, and applications. Physical Review Materials **6**(9), 090201 (2022)

Appendix- A1

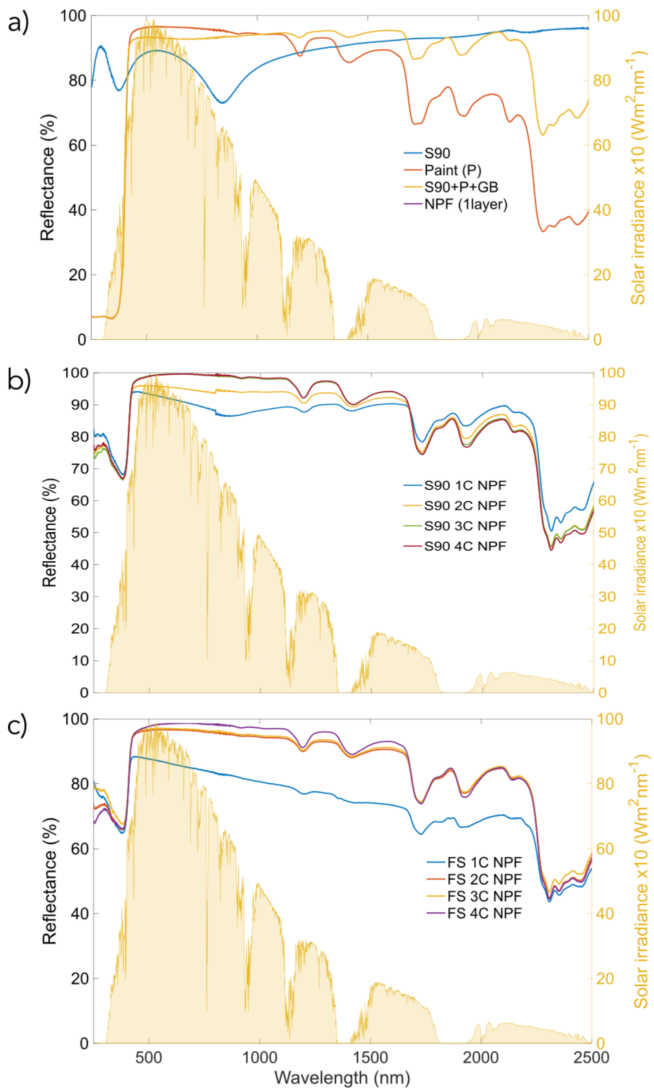

Fig. A1 Reflectance data for a) S90 substrate, ThermoShield paint, paint with the glass bubbles applied on the S90; b) S90 substrate covered with an increasing number of paint coats with the NPF applied to their top; c) the paint formulation with the NPF layer measures in a free-standing (FS) condition. In both previous panels the second y axis refers to the ASTM G173 solar irradiance.

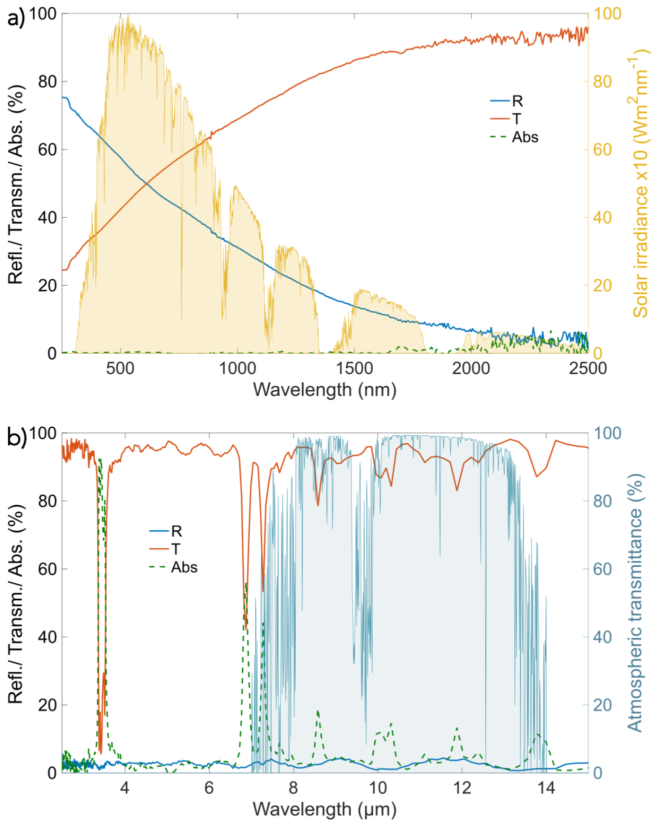

Fig. A2 Reflectance, Transmittance and Absorbance (emissivity) about NPF layer in a) solar spectrum from 250 nm to 2500 nm and in the IR spectrum from 2.5 μm to 15 μm

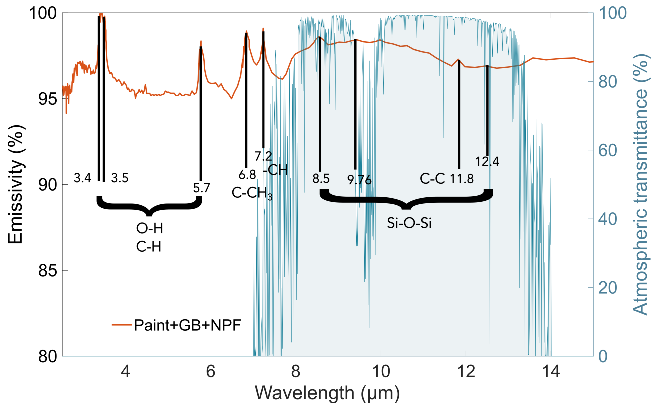

Fig. A3 Zoomed image of the FTIR analysis on the Paint + GB + NPF highlighting the main peaks in the IR spectrum.